

A Robust Distance Measurement and Dark Energy Constraints from the Spherically-Averaged Correlation Function of Sloan Digital Sky Survey Luminous Red Galaxies

Chia-Hsun Chuang^{*}, Yun Wang, and Maddumage Don P. Hemantha

Homer L. Dodge Department of Physics & Astronomy, Univ. of Oklahoma, 440 W Brooks St., Norman, OK 73019, U.S.A.

29 February 2012

ABSTRACT

We measure the effective distance to $z = 0.35$, $D_V(0.35)$ from the overall shape of the spherically-averaged two-point correlation function of the Sloan Digital Sky Survey (SDSS) Data Release 7 (DR7) luminous red galaxy (LRG) sample. We find $D_V(0.35) = 1428^{+74}_{-73}$ without assuming a dark energy model or a flat Universe. We find that the derived measurement of $r_s(z_d)/D_V(0.35) = 0.1143 \pm 0.0030$ (the ratio of the sound horizon at the drag epoch to the effective distance to $z = 0.35$) is more tightly constrained and more robust with respect to possible systematic effects. It is also nearly uncorrelated with $\Omega_m h^2$.

Combining our results with the cosmic microwave background and supernova data, we obtain $\Omega_k = -0.0032^{+0.0074}_{-0.0072}$ and $w = -1.010^{+0.046}_{-0.045}$ (assuming a constant dark energy equation of state). By scaling the spherically-averaged correlation function, we find the Hubble parameter $H(0.35) = 83^{+13}_{-15} \text{ km s}^{-1} \text{ Mpc}^{-1}$ and the angular diameter distance $D_A(0.35) = 1089^{+93}_{-87} \text{ Mpc}$.

We use LasDamas SDSS mock catalogs to compute the covariance matrix of the correlation function, and investigate the use of lognormal catalogs as an alternative. We find that the input correlation function can be accurately recovered from lognormal catalogs, although they give larger errors on all scales (especially on small scales) compared to the mock catalogs derived from cosmological N-body simulations.

Key words: cosmology: observations, distance scale, large-scale structure of Universe

1 INTRODUCTION

Galaxy redshift surveys provide a cosmological probe highly complementary to the cosmic microwave background (CMB) (Penzias & Wilson 1965) and supernovae (SNe) (Riess et al. 1998; Perlmutter et al. 1999). Large-scale structure data from galaxy surveys can be analyzed using either the power spectrum analysis or the correlation function analysis. Although these two methods are simple Fourier transforms of one another, the analysis processes are quite different and the results cannot be converted with Fourier transform directly because of the finite size of the survey volume. The SDSS data have been analyzed using both the power spectrum method (see, e.g., Tegmark et al. 2004; Hutsi 2005; Padmanabhan et al. 2007; Blake et al. 2007; Percival et al. 2007, 2010; Reid et al. 2010), and the correlation function method (see, e.g., Eisenstein et al. 2005; Okumura et al. 2008;

Cabre & Gaztanaga 2008; Martinez et al. 2009; Sanchez et al. 2009; Kazin et al. 2010).

The three major uncertainties while constructing a theoretical prediction of the power spectrum or correlation function with a given cosmological model are the galaxy bias (the relationship between galaxy and matter distributions), non-linear effects, and redshift distortions. The knowledge of these uncertainties determines which analysis method and scale range we should use to obtain reliable constraints on the dark energy and cosmological parameters.

In this paper, we present the measurement of the spherically-averaged correlation function from the SDSS DR7 luminous red galaxy (LRG) (Eisenstein et al. 2001; Abazajian et al. 2009) sample which provides a homogeneous galaxy sample and has the largest effective survey volume to date for studying the linear regime (Eisenstein et al. 2005). In Section 2, we introduce the galaxy sample and selection functions used in this study. In Section 3, we describe the details of our method. In Sec. 4, we present our results. In Sec. 5, we check our results using systematic tests. We summarize and conclude in Sec. 6.

^{*} E-mail: chuang@nhn.ou.edu

2 DATA

The SDSS has observed one-quarter of the entire sky and performed a redshift survey of galaxies, quasars and stars in five passbands u, g, r, i , and z with a 2.5m telescope (Fukugita et al. 1996; Gunn et al. 1998, 2006). We use the public catalog, the NYU Value-Added Galaxy Catalog (VAGC) (Blanton et al. 2005), derived from the SDSS II final public data release, Data Release 7 (DR7) (Abazajian et al. 2009). We select our LRG sample from the NYU VAGC with the flag *primTarget* bit mask set as 32. K-corrections have been applied to the galaxies with a fiducial model (Λ CDM with $\Omega_m = 0.3$ and $h = 1$), and the selected galaxies are required to have rest-frame g -band absolute magnitudes $-23.2 < M_g < -21.2$ (Blanton & Roweis 2007). The same selection criteria were used in previous work (Zehavi et al. 2005; Eisenstein et al. 2005; Okumura et al. 2008; Cabre & Gaztanaga 2008; Kazin et al. 2010). The sample we use is referred to as “DR7full” in Kazin et al. (2010). Our sample includes 87000 LRGs in the redshift range 0.16-0.44. The average weighted redshift of the sample is 0.33.

Spectra cannot be obtained for objects closer than 55 arcsec within a single spectroscopic tile due to the finite size of the fibers. To correct for these “collisions”, the redshift of an object that failed to be measured would be assigned to be the same as the nearest successfully observed one (Zehavi et al. 2005). Both fiber collision corrections and K-corrections have been made in NYU-VAGC (Blanton et al. 2005).

We have applied evolutionary correction based on the stellar synthesis model of an old and passively evolving burst from $z = 10$ by using the PEGASE code (Fioc & Rocca-Volmerange 1997). The rest-frame g -band absolute magnitudes are passively evolved to $z = 0.3$ (see Zehavi et al. (2005); Eisenstein et al. (2005)).

We construct the radial selection function as a cubic spline fit to the observed number density histogram with the width $\Delta z = 0.01$ (see Fig. 1). The NYU-VAGC provides the description of the geometry and completeness of the survey in terms of spherical polygons. Although the completeness of VAGC is determined based on the main galaxies (Strauss et al. 2002), we adopt it as the angular selection function of our sample since the main galaxies and LRGs should have similar angular selection functions (see the appendix of Zehavi et al. 2005). We drop the regions with completeness below 60% to avoid unobserved plates (Zehavi et al. 2005). The Southern Galactic Cap region is also dropped.

3 METHODOLOGY

In this section, we describe the measurement of the correlation function from the observational data, construction of the theoretical prediction, and the likelihood analysis that leads to constraints on dark energy and cosmological parameters. We will also show that using one scaling parameter is sufficient for extracting information from the observed spherically averaged correlation function (see Sec. 3.4.3).

3.1 Measuring the Two-point Correlation Function

We calculate the comoving distances to every galaxy by assuming a fiducial model, Λ CDM with $\Omega_m = 0.25$. We use the two-point correlation function estimator given by Landy and Szalay (Landy & Szalay 1993):

$$\xi(s) = \frac{DD(s) - 2DR(s) + RR(s)}{RR(s)}, \quad (1)$$

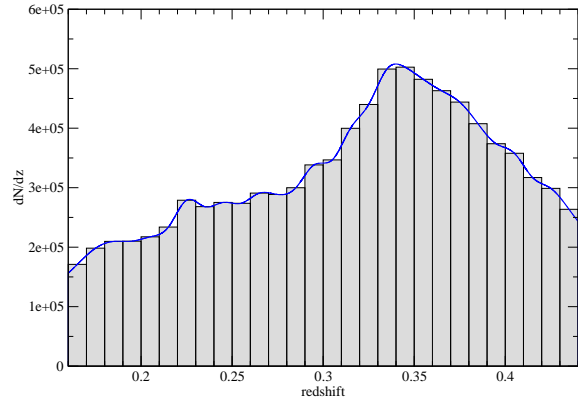


Figure 1. The radial selection function of the LRG sample used in this study. The gray bars are computed from the sample and the blue line is the cubic spline fit of these bar values. We compute the radial selection function in the form of the number of galaxies per unit redshift instead of the number density in comoving coordinate, so that we don’t need to assume a fiducial model while generating the random catalog with the radial selection function.

where DD, DR, and RR represent the normalized data-data, data-random, and random-random pair counts respectively in a distance range. The bin size we use in this study is $5h^{-1}\text{Mpc}$. This estimator has minimal variance for a Poisson process. Random data should be generated according to the radial and angular selection functions of the data. One can reduce the shot noise due to random data by increasing the number of random data. The number of random data we use is 10 times that of the real data. While calculating the pair counts, we assign each data point a radial weight of $1/[1 + n(z) \cdot P_w]$, where $n(z)$ is the radial selection function and $P_w = 4 \cdot 10^4 h^{-3}\text{Mpc}^3$ as in Eisenstein et al. (2005). The observed correlation function is shown in Fig. 2.

3.2 Theoretical Two-Point Correlation Function

We compute the linear power spectra at $z = 0.33$ by using CAMB (Lewis, Challinor, & Lasenby 2000). To include the damping effect of non-linear structure formation and peculiar velocities, we calculate the dewiggled power spectrum

$$P_{dw}(k) = P_{lin}(k) \exp\left(-\frac{k^2}{2k_*^2}\right) + P_{nw}(k) \left[1 - \exp\left(-\frac{k^2}{2k_*^2}\right)\right], \quad (2)$$

where $P_{lin}(k)$ is the linear power spectrum, $P_{nw}(k)$ is the no-wiggle or pure CDM power spectrum calculated with Eq.(29) in Eisenstein & Hu (1998), and k_* is marginalized over with a flat prior over the range of 0.09 to 0.13¹

We then use the software package *halofit* (Smith et al. 2003) to compute the non-linear matter power spectrum:

$$r_{halofit}(k) \equiv \frac{P_{halofit,nw}(k)}{P_{nw}(k)} \quad (3)$$

¹ Although k_* can be computed by renormalization perturbation theory (Crocce & Scoccimarro 2006; Matsubara 2007), doing so requires knowing the amplitude of the power spectrum, which is also marginalized over in this study.

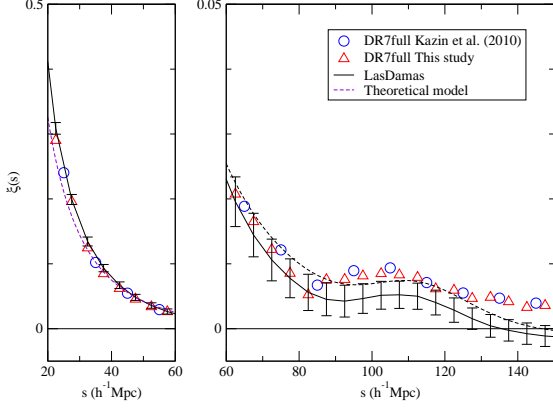


Figure 2. The spherically-averaged two-point correlation function measured from the SDSS DR7 data. The red triangles are the correlation function computed with the LRG sample described in Sec. 2. The green circles are taken from Kazin et al. 2010 in which the same fiducial model is used (Λ CDM with $\Omega_m = 0.25$) but the bin size they use is $10h^{-1}\text{Mpc}$. Our result shows excellent agreement with that of Kazin et al. 2010. The black line is the average correlation function from LasDamas mock catalogs. The error bars are the square roots of the diagonal elements of the covariance matrix we have derived (see Sec. 3.3). The violet dashed line is the mean model from our MCMC likelihood analysis ($\Omega_m h^2 = 0.105$, $\Omega_b h^2 = 0.0225$, $n_s = 0.978$, $D_V(0.35) = 1428\text{Mpc}$). Note that an MCMC analysis does not result in an accurate bestfit model (Lewis & Bridle 2002).

$$P_{nl}(k) = P_{dw}(k)r_{halofit}(k), \quad (4)$$

where $P_{halofit, nw}(k)$ is the power spectrum from applying *halofit* on the no-wiggle power spectrum and $P_{nl}(k)$ is the non-linear power spectrum. We compute the theoretical two-point correlation function by Fourier transforming the non-linear power spectrum. We show an example of the effect of applying dewiggle and *halofit* to the correlation function in Fig. 3. Clearly, the damping of the baryon acoustic oscillation (BAO) peak is accurately described by the dewiggled linear correlation function. Additional nonlinear effects are only important on very small scales.

The parameter set we use to compute the theoretical correlation function is $\{D_V(z), \Omega_m h^2, \Omega_b h^2, n_s, k_*, \kappa\}$, where Ω_m and Ω_b are the density fractions of matter and baryons, n_s is the power law index of the primordial matter power spectrum, h is the dimensionless Hubble constant ($H_0 = 100h \text{ km s}^{-1}\text{Mpc}^{-1}$), and $D_V(z)$ is defined by

$$D_V(z) \equiv \left[(1+z)^2 D_A^2 \frac{cz}{H(z)} \right]^{\frac{1}{3}}, \quad (5)$$

where $H(z)$ and $D_A(z)$ are the Hubble parameter and the angular diameter distance at the redshift, z . We set $h = 0.7$ while calculating the non-linear power spectra. Assuming the true model of our universe is not far from a Λ CDM model, the dark energy and curvature dependence are absorbed by the effective distance, $D_V(z)$. Thus we are able to extract constraints from data without assuming a dark energy model and cosmic curvature.

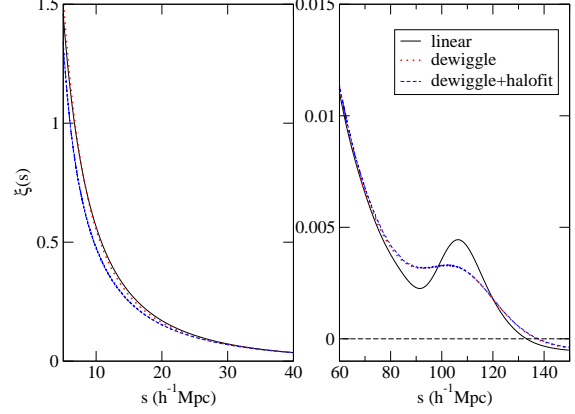


Figure 3. An example of the effect of applying dewiggle and *halofit* to the correlation function. The black solid line is the linear correlation function without applying dewiggle and *halofit* yet. The red dotted line is the dewiggled linear correlation function. The green dashed line is the dewiggled correlation function including nonlinear effects calculated using *halofit*. The damping of BAO is accurately described by the dewiggled linear correlation function. Additional nonlinear effects are only important on very small scales.

3.3 Covariance Matrix

We use the mock catalogs from the LasDamas simulations² (McBride et al., in preparation) to estimate the covariance matrix of the observed correlation function. LasDamas provides mock catalogs matching SDSS main galaxy and LRG samples. We use the LRG mock catalogs from the LasDamas gamma release with the same cuts as the SDSS LRGfull sample, $-23.2 < M_g < -21.2$ and $0.16 < z < 0.44$. We have diluted the mock catalogs to match the radial selection function of the observed data by randomly selecting the mock galaxies according to the number density of the data sample. We calculate the spherical-averaged correlation functions of the mock catalogs and construct the covariance matrix as

$$C_{ij} = \frac{1}{N-1} \sum_{k=1}^N (\bar{\xi}_i - \xi_i^k)(\bar{\xi}_j - \xi_j^k), \quad (6)$$

where N is the number of the mock catalogs, $\bar{\xi}_m$ is the mean of the m^{th} bin of the mock correlation functions, and ξ_m^k is the value of m^{th} bin of the k^{th} mock correlation function. We test the normality of the correlation functions from the LasDamas mock catalogs and find that they are well described by normal distributions (see Appendix B).

The mock catalogs derived from N-body simulations require long computing times and are very limited in availability. It is interesting to investigate whether there is an easier, faster, and cheaper way to construct mock catalogs which could work as well as those derived from N-body simulation. Towards this end, we have created 500 lognormal(LN) mock catalogs (Coles & Jones 1991; Percival, Verde, & Peacock 2004), and computed the spherically-averaged correlation functions from these. The details involved in creating LN mock catalogs are described in Appendix A. We compare the correlation functions from the LasDamas mock catalogs

² <http://lss.phy.vanderbilt.edu/lasdmas/>

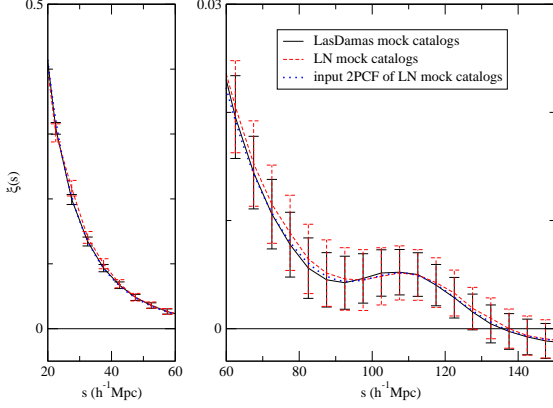


Figure 4. Spherical-averaged 2PCF of the mock catalogs. The black solid line is computed from the LasDamas mock catalogs. The red dashed line is computed from our lognormal mock catalogs. The error bars are the square roots of the diagonal elements of the covariance matrices. The green dotted line is the input 2PCF for our lognormal mock catalogs.

and LN mock catalogs in Fig. 4; the error bars indicate the square roots of the diagonal elements of the covariance matrices. We also show the normalized covariance matrices in Fig. 5 and 6. Clearly, the results from the LasDamas mocks and our LN mocks are very similar to each other. In particular, the input correlation function is accurately recovered by analyzing the LN mock catalogs. Note that the LN mocks give larger errors on all scales, and on scales smaller than $\sim 40 h^{-1} \text{Mpc}$, the LN mock catalogs give much larger errors than the LasDamas mock catalogs (see Fig. 7).

We use the covariance matrix computed from the LasDamas SDSS mock catalogs, since these are more realistic than the lognormal mock catalogs, and give smaller errors for the measured correlation function. It is interesting to note that in the absence of mock catalogs derived from cosmological N-body simulations, lognormal catalogs can be used for a conservative estimate of the covariance matrix of the correlation function.

3.4 Likelihood

The likelihood is taken to be proportional to $\exp(-\chi^2/2)$, and χ^2 is given by

$$\chi^2 \equiv \sum_{i,j=1}^{N_{bins}} [\xi_{th}(s_i) - \xi_{obs}(s_i)] C_{ij}^{-1} [\xi_{th}(s_j) - \xi_{obs}(s_j)] \quad (7)$$

where N_{bins} is the number of bins used, ξ_{th} is the theoretical correlation function of a model, and ξ_{obs} is the observed correlation function. Note that $\xi_{th}(s_i)$ depends on $\{D_V(z), \Omega_m h^2, \Omega_b h^2, n_s, k_*, \dots\}$.

In principle, we should recalculate the observed correlation function while computing the χ^2 for different models. However, since we don't consider the entire scale range of the correlation function (we only consider $s = 40 - 120 h^{-1} \text{Mpc}$ in this study), we might include or exclude different data pairs for different models which would render χ^2 values arbitrary. Therefore, instead of recalculating the observed correlation function, we apply the inverse operation to the theoretical correlation function to move the

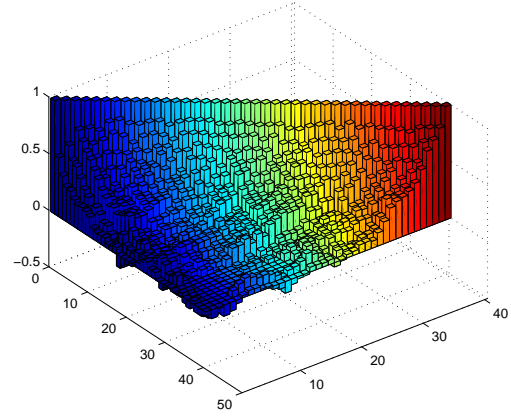


Figure 5. The normalized covariance matrix computed from 160 LasDamas mock catalogs. We show the covariance among 40 bins from $0 < s < 200 h^{-1} \text{Mpc}$ with bin size $5 h^{-1} \text{Mpc}$.

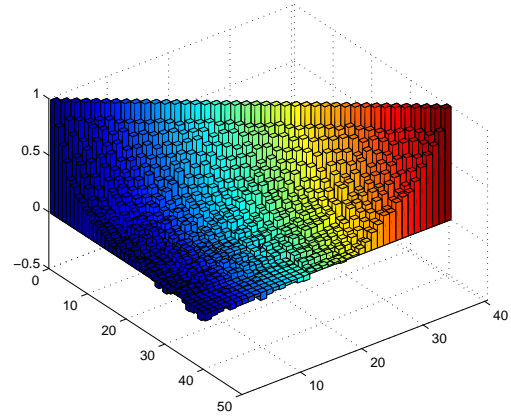


Figure 6. The normalized covariance matrix computed from 500 lognormal mock catalogs. We show the covariance among 40 bins between the scale range, $0 < s < 200 h^{-1} \text{Mpc}$, with the bin size, $5 h^{-1} \text{Mpc}$.

parameter dependence from the data to the model, thus preserving the number of galaxy pairs used in the likelihood analysis.

Let us define T as the operator converting the measured correlation function from the fiducial model to another model, i.e.,

$$\xi_{obs}(s) = T(\xi_{obs}^{fid}(s)). \quad (8)$$

where $\xi_{obs}^{fid}(s)$ is the observed correlation function assuming the fiducial model. This allows us to rewrite χ^2 as

$$\chi^2 \equiv \sum_{i,j=1}^{N_{bins}} \{T^{-1}[\xi_{th}(s_i)] - \xi_{obs}^{fid}(s_i)\} C_{fid,ij}^{-1} \cdot \{T^{-1}[\xi_{th}(s_j)] - \xi_{obs}^{fid}(s_j)\}, \quad (9)$$

where we have used Eqs.(6) and (8).

To find the operator T , note that the fiducial model is only used in converting redshifts into distances for the galaxies in our data sample. In the analysis of galaxy clustering, we only need the separation of a galaxy pair, and not the absolute distances to the galaxies. For a thin redshift shell, we can convert the separation of

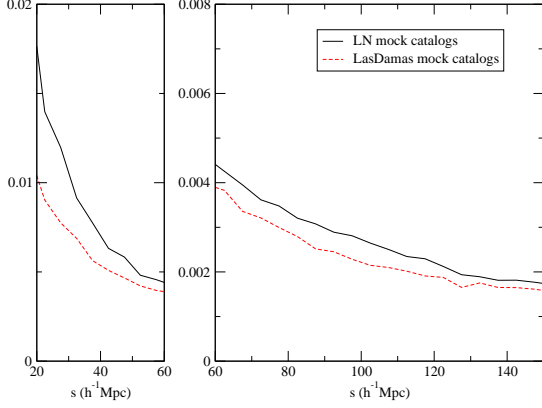


Figure 7. Square roots of the diagonal elements of the covariance matrices. The black dashed line is computed from the LasDamas mock catalogs. The red solid line is computed from lognormal mock catalogs we create. One can see that LN mock catalogs have larger covariance at smaller scale and two lines are close at larger scale.

one pair of galaxies from the fiducial model to another model by performing the scaling (see, e.g., Seo & Eisenstein (2003))

$$s' = \sqrt{\left(s \cos \theta \frac{H^{fid}(z)}{H(z)}\right)^2 + \left(s \sin \theta \frac{D_A(z)}{D_A^{fid}(z)}\right)^2}, \quad (10)$$

where θ is the angle between the radial direction and the direction of the line connecting the pair of galaxies.

Eisenstein et al. (2005) argued that we can use one rescaling parameter, $D_V(z)$, to convert the observed correlation function from the fiducial model to another model as long as the new model is not very different from the fiducial one, and the redshift range of the sample is not large. Then the separation of one pair of galaxies is converted from the fiducial model to another by

$$s' = \frac{D_V(z)}{D_V^{fid}(z)} s. \quad (11)$$

In this section, we discuss methods with one and two rescaling parameters, and show that these two methods are equivalent for spherically-averaged data when certain conditions hold (see Sec. 3.4.3).

3.4.1 Using One Rescaling Parameter

From eq. (11), the observed correlation function with the different model can be written as follows:

$$\xi_{obs}(s) = \xi_{obs}^{fid} \left(\frac{D_V^{fid}(z_{eff})}{D_V(z_{eff})} s \right), \quad (12)$$

where z_{eff} is the effective redshift of the sample and $D_V(z)$ is defined by Eq.(5).

The effective redshift we use in this study is $z_{eff} = 0.33$. Since the results are insensitive to z_{eff} (see Sec. 5), we rescale our result to $z_{eff} = 0.35$ for comparing with previous works. Eq. (12) can be rewritten as

$$\xi_{obs}^{fid}(s) = T^{-1}(\xi_{obs}(s)) = \xi_{obs} \left(\frac{D_V(z_{eff})}{D_V^{fid}(z_{eff})} s \right). \quad (13)$$

We can apply the same inverse rescaling operation to the theoretical correlation function:

$$T^{-1}(\xi_{th}(s)) = \xi_{th} \left(\frac{D_V(z_{eff})}{D_V^{fid}(z_{eff})} s \right). \quad (14)$$

χ^2 can be calculated by substituting eq. (14) into eq. (9).

3.4.2 Using Two Rescaling Parameters

From eq. (10), we can convert the spherically-averaged correlation function from some model to the fiducial model by

$$\begin{aligned} \xi_{obs}^{fid}(s) &= T^{-1}(\xi_{obs}(s)) \\ &= \int_0^\pi d\theta w(s, \theta) \times \\ &\quad \xi_{obs} \left(\sqrt{\left(s \cos \theta \frac{H^{fid}(z)}{H(z)}\right)^2 + \left(s \sin \theta \frac{D_A(z)}{D_A^{fid}(z)}\right)^2} \right), \end{aligned} \quad (15)$$

where the weighting function $w(r, \theta)$ is given by

$$w(s, \theta) = \frac{n_{DD}(s, \theta)}{\int_0^\pi d\theta n_{DD}(s, \theta)}, \quad (16)$$

where $n_{DD}(s, \theta)$ is the number density of the data pairs. We define inverse operation, T^{-1} , directly since T is not necessary in our calculation. We now apply the inverse operation to the theoretical correlation function:

$$\begin{aligned} T^{-1}(\xi_{th}(s)) &= \int_0^\pi d\theta w(s, \theta) \times \\ &\quad \xi_{th} \left(\sqrt{\left[s \cos \theta \frac{H^{fid}(z)}{H(z)}\right]^2 + \left[s \sin \theta \frac{D_A(z)}{D_A^{fid}(z)}\right]^2} \right). \end{aligned} \quad (17)$$

χ^2 can be calculated by substituting eq. (17) into eq. (9).

3.4.3 Equivalence of Using One and Two Rescaling Parameters for Spherically-Averaged Data

We now show that using one and two rescaling parameters while calculating the spherically-averaged correlation function are equivalent to first order in approximation. If the size of the survey is much larger than the scales of interest, $n_{DD}(s, \theta)$ would be proportional to $s \sin \theta$. Hence

$$w(s, \theta) \sim \frac{s \sin \theta}{\int_0^\pi s \sin \theta d\theta} = \frac{\sin \theta}{2}. \quad (18)$$

Next, if the model is close to the fiducial model, we can just consider the first order terms of D_V/D_V^{fid} , H^{fid}/H , and D_A/D_A^{fid} which can be written as following:

$$\frac{D_V}{D_V^{fid}} \simeq 1 + \delta_V, \quad \frac{H^{fid}}{H} \simeq 1 + \delta_r, \quad \frac{D_A}{D_A^{fid}} \simeq 1 + \delta_a, \quad (19)$$

where $|\delta_V|, |\delta_r|, |\delta_a| \ll 1$. From the definition of D_V (see Eq.(5)), one can obtain a simple relation, $3\delta_V \simeq \delta_r + 2\delta_a$. Let's consider a power law correlation function:

$$\xi_{th}(s) = s^p, \quad (20)$$

where p is a real number. Eq.(17) can be rewritten as

$$\begin{aligned}
& T^{-1}(\xi_{th}(s)) \\
& \simeq \int_0^\pi d\theta \frac{\sin \theta}{2} \left(\sqrt{[s \cos \theta (1 + \delta_r)]^2 + [s \sin \theta (1 + \delta_a)]^2} \right)^p \\
& \simeq \frac{s^p}{2} \int_0^\pi d\theta \sin \theta [\cos^2 \theta (1 + 2\delta_r) + \sin^2 \theta (1 + 2\delta_a)]^{\frac{p}{2}} \\
& \simeq \frac{s^p}{2} \int_0^\pi d\theta \sin \theta [1 + p(\cos^2 \theta \delta_r + \sin^2 \theta \delta_a)] \\
& = s^p \left[1 + p \frac{\delta_r + 2\delta_a}{3} \right] \\
& \simeq s^p (1 + p\delta_V) \\
& \simeq \left(\frac{D_V}{D_V^{fid}} s \right)^p \\
& = \xi_{th} \left(\frac{D_V}{D_V^{fid}} s \right)
\end{aligned} \tag{21}$$

The proof can be generalized to any function which can be expressed as

$$\xi_{th}(s) = s^{p_1} + s^{p_2} + s^{p_3} + \dots \tag{22}$$

where p_i are real numbers.

To measure the spherically-averaged correlation function, we have shown that using one rescaling parameter, D_V , and two rescaling parameters, H and D_A , are equivalent as long as the scales of interest are relatively small compared to the survey length scale, and the constraint on D_V is tight enough. A similar statement can be made for the spherically-averaged power spectrum analysis. We have verified that these two rescaling methods give similar results.

3.5 Markov Chain Monte-Carlo Likelihood Analysis

We use CosmoMC (Lewis & Bridle 2002) in a Markov Chain Monte-Carlo likelihood analysis. The main parameter space that we explore is $\{\Omega_m h^2, \Omega_b h^2, n_s, D_V(z_{eff}), k_*\}$ and the prior ranges are $\{(0.025, 0.3), (0.01859, 0.02657), (0.865, 1.059), (725, 1345), (0.09, 0.13)\}$ respectively. The dependence on h , the curvature, and dark energy parameters are absorbed into $D_V(z_{eff})$.

We marginalize over the amplitude of the correlation function; this is equivalent to marginalizing over galaxy bias $\times \sigma_8 \times r_\beta$, where σ_8 is the matter power spectrum normalization parameter and r_β is the linear ratio between the correlation function in the redshift space and real space which can be derived from the linear redshift distortion parameter (Kaiser 1987). Since the LRG data alone cannot give tight constraints on $\Omega_b h^2$ and n_s , we apply flat priors ($\pm 7\sigma_{WMAP7}$) on them which are wide enough so that CMB constraints will not be double counted. In other words, the effect from the wide flat priors could be ignored when combining our final results with CMB data. We also marginalized over k_* over the range of 0.09 to 0.13 (see Sec.3.2).

4 RESULTS

In this section, we present the model independent measurements of the parameters we explore, $\{D_V(0.35), \Omega_m h^2\}$, obtained by using the method described in previous sections. Although, the effective redshift we use is 0.33, the average weighted redshift, we rescale

all our results to $z_{eff} = 0.35$ for comparing with previous work easily by

$$D_V(0.35) = D_V(0.33) \frac{D_{V,fid}(0.35)}{D_{V,fid}(0.33)} = 1.054 D_V(0.33). \tag{23}$$

We have checked that the results is insensitive to the effective redshift in Sec. 5.

We derive the model independent measurements of H and D_A for comparison with 2D results. We also apply the method on two subsamples (two redshift slices) as a systematic test.

We validate our method by applying it to the LasDamas mock catalogs, and find that our measurements are consistent with the input parameters of the simulations.

We derive constraints on dark energy and cosmological parameters by combining our results with other data sets including WMAP7 (Komatsu et al. 2010) and Union2 SN (Amanullah et al. 2010).

Finally, we compare our results with previous works.

4.1 Model Independent Constraints on $D_V(0.35)$

Without assuming a dark energy model or a flat Universe, we find that $D_V(0.35) = 1428_{-73}^{+74}$ Mpc and $r_s(z_d)/D_V(0.35) = 0.1143 \pm 0.0030$, where $r_s(z_d)$ is the comoving sound horizon at the drag epoch calculated with the eq. (6) in Eisenstein & Hu (1998).

Fig. 8 shows one and two-dimensional marginalized contours of the parameters, $\{D_V(0.35), \Omega_m h^2, r_s(z_d)/D_V(0.35), A(0.35)\}$, where

$$A(z) \equiv D_V(z) \frac{\sqrt{\Omega_m H_0^2}}{cz}. \tag{24}$$

The measurements and the covariance matrix are listed in Table 1 and 2. The bestfit model from the MCMC likelihood analysis has $\chi^2 = 6.32$ for 16 bins of data used (in the scale range of $40 h^{-1} \text{Mpc} < s < 120 h^{-1} \text{Mpc}$ with the bin size = $5 h^{-1} \text{Mpc}$), for a set of 6 parameters (including the overall amplitude of the correlation function).

The scale range of the correlation function we have selected is $s = 40 - 120 h^{-1} \text{Mpc}$. In this range, the scale dependence of the redshift distortion and galaxy bias is small. We cut the tail of the correlation function at $s = 120 h^{-1} \text{Mpc}$ because the high tail (large correlation at large scales) cannot be fitted to any conventional model, and could be due to systematic error or sample variance (see further discussion in Sec. 5).

At this point, we assume the high tail is simply due to sample variance, and might disappear when much larger data sets become available. Unlike previous analyses by other groups, we apply very weak flat priors ($\pm 7\sigma_{WMAP7}$) on $\Omega_b h^2$ and n_s instead of fixing them to the bestfit values from CMB data.

4.2 Model independent measurements of $H(0.35)$ and $D_A(0.35)$

In this section, we apply the method with two scaling parameters described in sec 3.4.2 to measure H and D_A . The main parameter space that we explore is $\{\Omega_m h^2, \Omega_b h^2, n_s, H(z_{eff}), D_A(z_{eff}), k_*\}$ and the prior ranges are $\{(0.025, 0.3), (0.01859, 0.02657), (0.865, 1.059), (41, 123), (723, 1343), (0.09, 0.13)\}$ respectively. We obtain the model independent measurements, $H(0.35) = 83_{-15}^{+13} \text{ km s}^{-1} \text{Mpc}^{-1}$ and $D_A(0.35) = 1089_{-87}^{+93} \text{ Mpc}$, from the LRG data alone (see Table

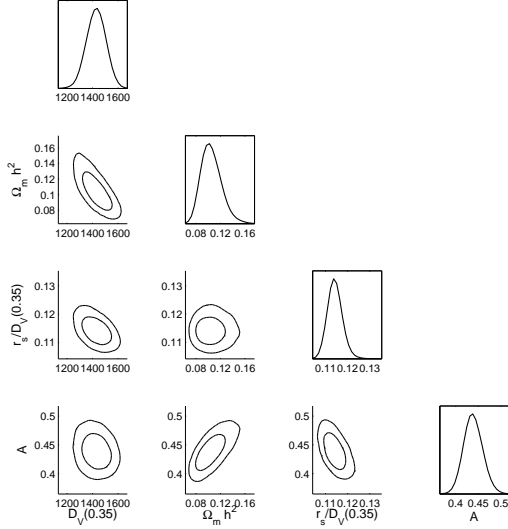


Figure 8. 2D marginalized contours (68% and 95% C.L.) for $D_V(0.35)$, $\Omega_m h^2$, $r_s(z_d)/D_V(0.35)$, and $A(0.35)$. The diagonal panels represent the marginalized probabilities.

	mean	σ	lower	upper
$D_V(0.35)(\text{Mpc})$	1428	74	1355	1502
$\Omega_m h^2$	0.105	0.016	0.090	0.121
$r_s(z_d)/D_V(0.35)$	0.1143	0.0033	0.1113	0.1173
$A(0.35)$	0.439	0.020	0.419	0.459

Table 1. Measured cosmological parameters with flat prior $0.01859 < \Omega_b h^2 < 0.02657$, $0.865 < n_s < 1.059$ ($\pm 7\sigma_{WMAP7}$), and $0.09 < k_* < 0.13h^{-1}/\text{Mpc}$. The standard deviations and the marginalized bounds (68%) are listed as well. There are two derived measurements, $r_s(z_d)/D_V(0.35)$ and $A(0.35)$, in the table.

3). Table 4 shows the normalized covariance matrix of $\{H(0.35), D_A(0.35), \Omega_m h^2, H(0.35)r_s(z_d), r_s(z_d)/D_A(0.35), A(0.35)\}$, and Fig. 9 shows the 2D marginalized contours of this parameter set.

Although using two rescaling parameters on the spherically-averaged correlation function cannot give better constraints on the cosmological parameters, it gives the model independent measurements of H and D_A which cannot be derived directly from the measurement of D_V . These can be compared to our result for the two-dimensional two-point correlation function (Chuang & Wang 2011), $H(0.35) = 82.1^{+4.8}_{-4.9} \text{ km s}^{-1} \text{ Mpc}^{-1}$ and $D_A(0.35) =$

	$D_V(0.35)$	$\Omega_m h^2$	$\frac{r_s(z_d)}{D_V(0.35)}$	$A(0.35)$
$D_V(0.35)$	1	-0.7890	-0.5561	-0.1727
$\Omega_m h^2$	-0.7890	1	0.0056	0.7305
$\frac{r_s(z_d)}{D_V(0.35)}$	-0.5561	0.0056	1	-0.6181
$A(0.35)$	-0.1727	0.7305	-0.6181	1

Table 2. Normalized covariance matrix with flat prior $0.01859 < \Omega_b h^2 < 0.02657$, $0.865 < n_s < 1.059$ ($\pm 7\sigma_{WMAP7}$), and $0.09 < k_* < 0.13h^{-1}/\text{Mpc}$.

	mean	σ	lower	upper
$H(0.35) (\text{km s}^{-1} \text{ Mpc}^{-1})$	83	17	68	96
$D_A(0.35) (\text{Mpc})$	1089	93	1002	1182
$\Omega_m h^2$	0.105	0.017	0.089	0.122
$H(0.35) * r_s(z_d)$	13500	2700	11200	15500
$r_s(z_d)/D_A(0.35)$	0.151	0.012	0.140	0.161
$A(0.35)$	0.432	0.026	0.408	0.457

Table 3. Measured cosmological parameters with flat prior $0.01859 < \Omega_b h^2 < 0.02657$, $0.865 < n_s < 1.059$ ($\pm 7\sigma_{WMAP7}$), and $0.09 < k_* < 0.13h^{-1}/\text{Mpc}$. The standard deviations and the marginalized bounds (68%) are listed as well. There are three derived measurements, $H(0.35) * r_s(z_d)$, $r_s(z_d)/D_A(0.35)$, and $A(0.35)$, in the table.

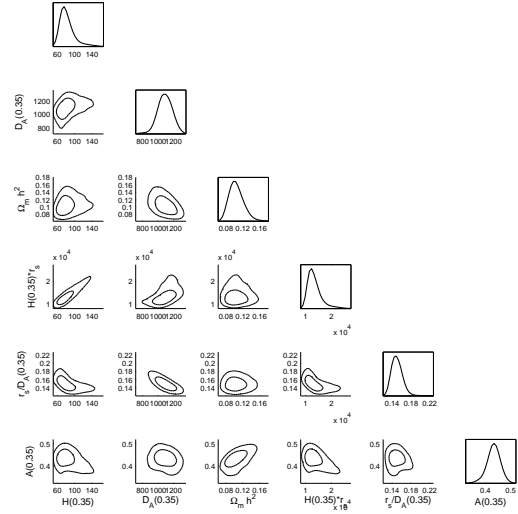


Figure 9. 2D marginalized contours for 68% and 95% for $H(z = 0.35)$, $D_A(z = 0.35)$, $\Omega_m h^2$, $H(0.35) * r_s(z_d)$, $r_s(z_d)/D_A(0.35)$, and $A(0.35)$. The diagonal panels represent the marginalized probabilities.

$1048^{+60}_{-58} \text{ Mpc}$. Not surprisingly, information is lost in the spherical averaging of data.

4.3 Model independent measurements of $r_s(z_d)/D_V(z)$ from two redshift slices

To explore the redshift dependency of the measurements. We apply the method of one rescaling parameter on two subsamples have $z = 0.16 - 0.36$ and $z = 0.28 - 0.44$. The average weighted redshifts of these two samples are 0.28 and 0.36 respectively. Both subsamples have ~ 60000 galaxies. We find $r_s(z_d)/D_V(0.28) = 0.141 \pm 0.012$ and $r_s(z_d)/D_V(0.36) = 0.1146 \pm 0.0068$. Because of the overlapping of the samples, there is covariance between these two measurements. To estimate the covariance, we apply the method on 40 mock catalogs (indexed from 01a to 40a) and find the correlation coefficient $r = 0.20$. To combine these measurements with other data sets, one should add the following term to the χ^2 :

$$\chi^2_{LRG2Z} = \Delta_{LRG2Z} \begin{pmatrix} 6688 & -2437 \\ -2437 & 22200 \end{pmatrix} \Delta_{LRG2Z} \quad (25)$$

where

$$\Delta_{LRG2Z} = \begin{pmatrix} r_s(z_d)/D_A(0.28) - 0.1413 \\ r_s(z_d)/D_A(0.36) - 0.1146 \end{pmatrix} \quad (26)$$

	$H(0.35)$	$D_A(0.35)$	$\Omega_m h^2$	$H(0.35) * r_s(z_d)$	$r_s(z_d)/D_A(0.35)$	$A(0.35)$
$H(0.35)$	1	0.4028	0.2133	0.9744	-0.5733	-0.3460
$D_A(0.35)$	0.4028	1	-0.4829	0.5300	-0.8440	-0.1210
$\Omega_m h^2$	0.2133	-0.4829	1	0.0025	-0.0139	0.6035
$H(0.35) * r_s(z_d)$	0.9744	0.5300	0.0025	1	-0.5861	-0.4723
$r_s(z_d)/D_A(0.35)$	-0.5733	-0.8440	-0.0139	-0.5861	1	-0.2033
$A(0.35)$	-0.3460	0.0908	0.6035	-0.4723	-0.2033	1

Table 4. Normalized covariance matrix with flat prior $0.01859 < \Omega_b h^2 < 0.02657$, $0.865 < n_s < 1.059 (\pm 7\sigma_{WMAP7})$, and $0.09 < k_* < 0.13h^{-1}/\text{Mpc}$.

The constraints of cosmological parameters from combining CMB and SNe data set for the Λ CDM model are shown in Table. 5. The measurements are similar to using the whole sample ($z=0.16-0.44$) but the constraints are worse. It might be due to some tension between the measurements of these two subsample which might be caused by higher noise level from smaller samples or by the evolution of the dark energy which would need a more complex model than Λ CDM. We will explore this issue in our future research.

4.4 Constraints on Λ CDM Model

We now present the cosmological parameter constraints for the Λ CDM model (non-flat Universe with a constant dark energy equation of state). Table. 5 also shows the constraints from cosmological microwave background (WMAP7) and supernova (Union2 compilation) data and their combination with SDSS LRG data. To include the constraints from WMAP7 (Komatsu et al. 2010), we use the constraints on the CMB shift parameters $\{R, l_a\}$ and z_* by Wang, Chuang, & Mukherjee (2011) (see Appendix C). To calculate the constraints from Union2 SNe, we use the add-on code for cosmoMC which can be download from the website of Union2 SNe³. For a given model, one could obtain χ^2 for each data set, i.e. χ^2_{CMB} and χ^2_{SN} ⁴. To include the constraint we obtained from the galaxy clustering data, one should add the following term to the χ^2 with

$$\chi^2_{LRG} = \left[\frac{r_s(z_d)/D_V(0.35) - 0.1143}{0.0033} \right]^2 \quad (27)$$

Combining all three data sets, LRG, CMB, and SNe, and assuming the Λ CDM model, we find that $\Omega_k = -0.0032^{+0.0074}_{-0.0072}$, and $w = -1.010^{+0.046}_{-0.045}$, which is consistent with Λ CDM model (in agreement with previous work, see e.g., Serra et al. 2009; Wang 2009; Mortonson, Hu, & Huterer 2010; Zhao & Zhang 2010). Fig. 10 compares the constraints on w and Ω_k in the Λ CDM model. We can see that the addition of SDSS LRG data significantly tightens the constraints on dark energy and cosmological parameters.

4.5 Validation Using Mock Catalogs

In order to validate our method, we have applied it to the 2D 2PCF of 40 LasDamas mock catalogs (which are indexed with 01a-40a). Again, we apply the flat and wide priors ($\pm 7\sigma_{WMAP7}$) on $\Omega_b h^2$

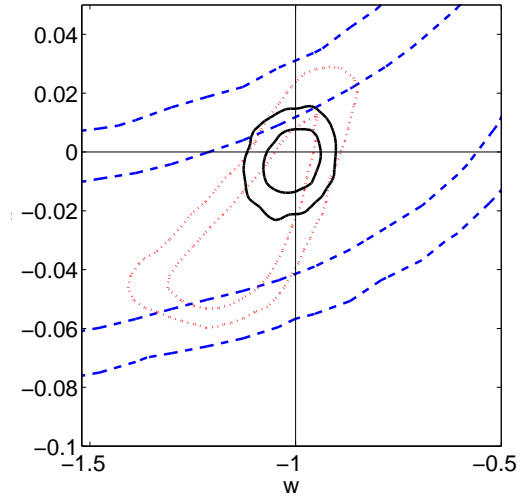


Figure 10. 2D marginalized contours for 68% and 95% for w and Ω_k (Λ CDM model assumed) from WMAP7 (dashed blue), WMAP7+Union2 SN (dotted red), and WMAP7+Union2 SN+LRG (solid black). The straight solid black lines indicate that $w = -1$ and $\Omega_k = 0$.

	mean	σ	input value
$D_V(0.35)(\text{Mpc})$	1349	69	1356
$\Omega_m h^2$	0.120	0.015	0.1225
$r_s(z_d)/D_V(0.35)$	0.1205	0.0059	0.1175
$A(0.35)$	0.441	0.026	0.452

Table 6. The mean, standard deviation, and the 68% C.L. bounds of $\{D_V(0.26), \Omega_m h^2, r_s(z_d)/D_V(0.35), A(0.35)\}$ from the LRGfull mock catalogs of the LasDamas simulations. Our measurements are consistent with the input values within 1σ .

and n_s , centered on the input values of the simulation ($\Omega_b h^2 = 0.0196$ and $n_s = 1$).

Table 6 shows our measurements of $\{D_V(0.35), \Omega_m h^2, r_s(z_d)/D_V(0.35), A(0.35)\}$ from the LasDamas mock catalogs of the SDSS LRG sample. These are consistent with the input parameters, establishing the validity of our method.

4.6 Comparison with other analyses

There have been several analyses of the clustering of the SDSS LRG spectroscopic sample. Percival et al. (2010) use power spectrum analysis to extract the BAO signals. The sample they use include not only LRGs but also main galax-

³ <http://supernova.lbl.gov/Union/>

⁴ While computing χ^2_{SN} , we use the covariance matrix with systematics to obtain more reliable constraints from SNe

	Ω_m	Ω_X	w	H_0	$\Omega_m h^2$	Ω_k
CMB	$0.325^{+0.072}_{-0.077}$	$0.67^{+0.073}_{-0.071}$	$-1.04^{+0.62}_{-0.63}$	$65.7^{+8.2}_{-7.2}$	$0.1356^{+0.0059}_{-0.0060}$	$0.006^{+0.058}_{-0.048}$
CMB+SN	$0.348^{+0.06}_{-0.072}$	$0.676^{+0.052}_{-0.045}$	-1.11 ± 0.11	$63.4^{+6.5}_{-5.8}$	$0.1361^{+0.0061}_{-0.0060}$	$-0.025^{+0.022}_{-0.019}$
CMB+SN+LRG	$0.279^{+0.018}_{-0.019}$	0.725 ± 0.018	$-1.01^{+0.046}_{-0.045}$	69.9 ± 2.3	$0.1357^{+0.0061}_{-0.0059}$	$-0.0032^{+0.0074}_{-0.0072}$
CMB+SN+LRG2Z	0.278 ± 0.032	0.725 ± 0.026	$-1.008^{+0.053}_{-0.054}$	70.3 ± 4.2	$0.136^{+0.0061}_{-0.0063}$	-0.003 ± 0.011

Table 5. Constraints of the cosmological parameters from various data combinations with Λ CDM model assumed, where LRG is using the fiducial result of this paper (eq. 27) and LRG2Z is using the measurements from two subsamples as described in Sec. 4.3. There are two inferred parameters, Ω_m and Ω_k , in this table.

ies sample. They obtain the constraint on $r_s/D_V(0.35) = 0.1097 \pm 0.0036$. Reid et al. (2010) apply power spectrum analysis on the reconstructed halo density field derived from SDSS DR7full (flux-limited LRG) sample. Their measurement of $r_s/D_V(0.35) = 0.1097^{+0.0039}_{-0.0042}$ ($k_{max} = 0.2$) which is similar to Percival et al. (2010). There is about 1σ difference between their results and ours. However, in Reid et al. (2010), they show a dependence on the minimum scales of the range, i.e. $r_s/D_V(0.35) = 0.1118^{+0.0043}_{-0.0046}$ ($k_{max} = 0.15$) and $r_s/D_V(0.35) = 0.1136^{+0.0070}_{-0.0072}$ ($k_{max} = 0.1$). Their results are more consistent with ours when a smaller k_{max} (i.e., a larger minimum scale) is used, which represents a more conservative choice for the scale range.

5 SYSTEMATIC TESTS

Table. 7 shows the systematic tests that we have done varying key assumptions made in our analysis. These include the range of scales used to calculate the correlation function, the nonlinear damping scale, an overall shift in the measured correlation function due to a systematic error.

We vary the effective redshift (from $z_{eff} = 0.33$ to $z_{eff} = 0.35$) used to calculate the theoretical model. We rescale the results to $z = 0.35$ for comparison and find that the results are insensitive to the effective redshift.

We also test the sensitivity of our results to the nonlinear damping scale, k_* . Although k_* can be predicted accurately in the real space (Croce & Scoccimarro 2006; Matsubara 2007), in the redshift space, it would also depend on the redshift distortions which cannot be well determined from the spherically-averaged correlation function. In table. 7, one can tell that the results are not sensitive to k_* .

In principle, the range of scales chosen for the analysis should be as large as possible, in order to derive the tightest constraints. However, we do not use the small scales ($s < 40 h^{-1}\text{Mpc}$), where the scale dependence of redshift distortion and galaxy bias are not negligible and cannot be accurately determined at present. According to Fig. 5 in Eisenstein et al. (2005), these effects are negligible at $s > 40 h^{-1}\text{Mpc}$. We vary the minimum scales used and find that the $r_s(z_d)/D_V(0.35)$ is insensitive to it but $\Omega_m h^2$ is not. This indicates the robustness of the measurement of $r_s(z_d)/D_V(0.35)$ (but not $\Omega_m h^2$) from this paper.

On larger scales ($s > 130 h^{-1}\text{Mpc}$), the observed correlation is significantly higher than expected in conventional models of galaxy clustering. This high tail problem was reported in previous work, see, e.g., Eisenstein et al. (2005), Hutsi (2005), and Sanchez et al. (2009). They found that the observed correlation function could be fitted better by lowering all the data points by a

constant. In other words, they assumed a constant shift from some systematic error. Although this systematic error is unknown, we could minimize its effect by using smaller scale. The reason is that the correlation function has larger value at smaller scale so that the results are less sensitive to the shift. We choose $s = 120 h^{-1}\text{Mpc}$ as our boundary for the large scale and show that the results are insensitive to the constant shift by lowering down the data points of the observed correlation function by 0.002. We find that $\Omega_m h^2$ varies by 1σ and $r_s/D_V(0.35)$ only varies by 0.2σ . Therefore, our measurement of $r_s/D_V(0.35)$ is robust to the systematic shift. This is another indication that our measurement of $r_s(z_d)/D_V(0.35)$ (but not that of $\Omega_m h^2$) is robust.

6 CONCLUSION

We have presented our first results for the model independent constraints on dark energy from the spherically-averaged correlation function of SDSS DR7 data, using an MCMC likelihood analysis. Our constraints on $\{D_V(0.35), \Omega_m h^2, r_s(z_d)/D_V(0.35), A(0.35)\}$ are summarized by Table 1 and 2. Applying these results to constraining a constant dark energy equation of state without assuming a flat Universe (the Λ CDM model), and combining with WMAP7 and Union2 SN data sets, we find that $\Omega_k = -0.0032^{+0.0074}_{-0.0072}$ and $w = -1.010^{+0.046}_{-0.045}$, consistent with a flat universe with a cosmological constant ($\Omega_k = 0, w = -1$).

We have also measured the model independent constraints of $H(0.35)$ and $D_A(0.35)$ from the spherically-averaged correlation function from SDSS DR7 LRGs, as a baseline for comparison with constraints from studies of the 2D correlation function (see Chuang & Wang (2011)). We find that $\{H(0.35), D_A(0.35)\}$ from the spherically-averaged correlation function provide much weaker constraints than the 2D correlation function; this is as expected since spherically-averaging reduces the amount of information extractable from data.

The correlation function analysis is expected to be a more robust way to extract the BAO signals than the power spectrum analysis, because one can easily get rid of the systematic uncertainties such as the redshift distortion, the galaxy bias, and the non-linear effect by cutting off the small scale range (Sanchez, Baugh, and Angulo 2008).

The power of the correlation function analysis is limited at present by the available data. The correlation function that we have measured from the SDSS DR7 data has a high tail (larger than expected correlations) at large scales ($s > 120$) (see Fig. 2). Whether this high tail is simply due to the sample variance or some other systematic issue, e.g., extinction correction, will only become clear

	$D_V(0.35)(\text{Mpc})$	$\Omega_m h^2$	$r_s(z_d)/D_V(0.35)$	$A(0.35)$
fiducial model	1428^{+74}_{-73}	0.105 ± 0.016	$0.1143^{+0.0029}_{-0.0031}$	0.439 ± 0.02
$z_{eff} = 0.35$	1427^{+72}_{-71}	$0.105^{+0.016}_{-0.015}$	$0.1144^{+0.0030}_{-0.0031}$	0.439 ± 0.02
$k_* = 0.11$	1426^{+73}_{-72}	0.106 ± 0.015	$0.1144^{+0.0030}_{-0.0031}$	0.439 ± 0.02
$s=20-120$	1398^{+64}_{-62}	0.116 ± 0.012	0.1139 ± 0.0028	0.453 ± 0.015
$s=60-120$	1418^{+94}_{-93}	0.108 ± 0.025	$0.1149^{+0.0030}_{-0.0033}$	0.438 ± 0.03
$s=40-100$	1448^{+96}_{-89}	$0.114^{+0.018}_{-0.019}$	$0.111^{+0.0050}_{-0.0058}$	$0.463^{+0.033}_{-0.032}$
$s=40-140$	1393^{+90}_{-87}	0.110 ± 0.018	$0.1164^{+0.0040}_{-0.0047}$	$0.437^{+0.025}_{-0.023}$
shift = 0.002	1388^{+80}_{-77}	0.122 ± 0.020	$0.1136^{+0.0032}_{-0.0035}$	0.459 ± 0.023

Table 7. This table shows the systematic tests with the scale range, the fiducial model used, the effective redshift, the damping factor, and the shift from a systematic error. The fiducial results is obtained by assuming Λ CDM model with $\Omega_m = 0.25$ as fiducial model considering the scale range ($s = 40 - 120 h^{-1}\text{Mpc}$), using the effective redshift ($z_{eff} = 0.33$), and the damping factor, k_* , marginalized over with the a flat prior ($0.09 < k_* < 0.13 h\text{Mpc}^{-1}$). The other results are calculated with only one quantity different from the fiducial one. $n_s = 0.963$ and $\Omega_b h^2 = 0.02258$ are marginalized with the same flat priors ($\pm 7\sigma_{WMAP7}$) in this paper.

as more ambitious galaxy survey data become available in the future (e.g., from BOSS⁵, or Euclid⁶).

ACKNOWLEDGEMENTS

We would like to thank Michael Blanton, Daniel Eisenstein, Alex Kim, Antony Lewis, Ariel Sanchez, and Martin White for useful comments. We are grateful to the LasDamas project for making their mock catalogs publicly available. The computing for this project was performed at the OU Supercomputing Center for Education and Research (OSKER) at the University of Oklahoma (OU). OSCER Director Henry Neeman and HPC Application Software Specialist Joshua Alexander provided invaluable technical support. This work was supported in part by DOE grant DE-FG02-04ER41305.

REFERENCES

Abazajian, K. N., *et al.* [SDSS Collaboration], *Astrophys. J. Suppl.* **182**, 543 (2009) [arXiv:0812.0649 [astro-ph]].
Amanullah, R., *et al.*, *Astrophys. J.* **716**, 712 (2010) [arXiv:1004.1711 [astro-ph.CO]].
Blake, C.; Collister, A.; Bridle, S.; and Lahav, O., *Mon. Not. Roy. Astron. Soc.* **374**, 1527 (2007) [arXiv:astro-ph/0605303].
Blanton, M. R., *et al.* [SDSS Collaboration], *Astron. J.* **129**, 2562 (2005) [arXiv:astro-ph/0410166].
Blanton, M. R.; and Roweis, S., *Astron. J.* **133**, 734 (2007) [arXiv:astro-ph/0606170].
Cabre, A.; and Gaztanaga, E., arXiv:0807.2460 [astro-ph].
C. H. Chuang and Y. Wang, arXiv:1102.2251 [astro-ph.CO].
Cimatti, A.; Robberto, M.; Baugh, C.; Beckwith, S. V. W.; Content, R.; Daddi, E.; De Lucia, G.; Garilli, B.; Guzzo, L.; Kauffmann, G.; Lehnert, M.; Maccagni, D.; Martinez-Sansigre, A.; Pasian, F.; Reid, I. N.; Rosati, P.; Salvaterra, R.; Stiavelli, M.; Wang, Y.; Osorio, M. Zapatero; the SPACE team, *Experimental Astronomy*, **23**, 39 (2009).
Coles, P., and Jones, B., *Mon. Not. Roy. Astron. Soc.* **248** (1991) 1.

M. Crocce and R. Scoccimarro, *Phys. Rev. D* **73**, 063520 (2006) [arXiv:astro-ph/0509419].
Eisenstein, D. J.; and Hu, W., *Astrophys. J.* **496**, 605 (1998) [arXiv:astro-ph/9709112].
Eisenstein, D. J., *et al.* [SDSS Collaboration], *Astron. J.* **122**, 2267 (2001) [arXiv:astro-ph/0108153].
Eisenstein, D. J., *et al.* [SDSS Collaboration], *Astrophys. J.* **633**, 560 (2005) [arXiv:astro-ph/0501171].
Eisenstein, D. J.; Seo, H. j.; and White, M. J., *Astrophys. J.* **664**, 660 (2007) [arXiv:astro-ph/0604361].
Fioc, M.; and Rocca-Volmerange, B., *Astron. Astrophys.* **326**, 950 (1997) [arXiv:astro-ph/9707017].
Fukugita, M.; Ichikawa, T.; Gunn, J. E.; Doi, M.; Shimasaku, K.; and Schneider, D. P., *Astron. J.* **111**, 1748 (1996).
Gunn, J. E., *et al.* [SDSS Collaboration], *Astron. J.* **116**, 3040 (1998) [arXiv:astro-ph/9809085].
Gunn, J. E., *et al.* [SDSS Collaboration], *Astron. J.* **131**, 2332 (2006) [arXiv:astro-ph/0602326].
Hemantha, M. D. P.; Wang, Y.; and Chuang, C., in preparation
W. Hu and N. Sugiyama, *Astrophys. J.* **471**, 542 (1996) [arXiv:astro-ph/9510117].
Hutsi, G., arXiv:astro-ph/0507678.
N. Kaiser, *Mon. Not. Roy. Astron. Soc.* **227**, 1 (1987).
Kazin, E. A., *et al.*, *Astrophys. J.* **710**, 1444 (2010) [arXiv:0908.2598 [astro-ph.CO]].
Komatsu, E., *et al.*, arXiv:1001.4538 [astro-ph.CO].
Landy, S. D.; and Szalay, A. S., *Astrophys. J.* **412**, 64 (1993).
Laureijs, R. *et al.* 2009, “Euclid Assessment Study Report for the ESA Cosmic Visions”, arXiv:0912.0914
Lewis, A.; Challinor, A.; and Lasenby, A., *Astrophys. J.* **538**, 473 (2000) [arXiv:astro-ph/9911177].
Lewis, A., and Bridle, S., *Phys. Rev. D* **66**, 103511 (2002) [arXiv:astro-ph/0205436].
Martinez, V. J., *et al.*, *Astrophys. J.* **696**, L93 (2009) [Erratum-ibid. **703**, L184 (2009)] [*Astrophys. J.* **703**, L184 (2009)] [arXiv:0812.2154 [astro-ph]].
T. Matsubara, *Phys. Rev. D* **77**, 063530 (2008) [arXiv:0711.2521 [astro-ph]].
Mortonson, M. J.; Hu, W.; Huterer, D., 2010, *PRD*, **81**, 063007
Okumura, T.; Matsubara, T.; Eisenstein, D. J.; Kayo, I.; Hikage, C.; Szalay, A. S.; and Schneider, D. P., *Astrophys. J.* **676**, 889 (2008) [arXiv:0711.3640 [astro-ph]].
Padmanabhan, N., *et al.* [SDSS Collaboration], *Mon. Not. Roy. Astron. Soc.* **378**, 852 (2007) [arXiv:astro-ph/0605302].

⁵ <http://www.sdss3.org/cosmology.php>

⁶ See <http://sci.esa.int/euclid>, and Cimatti *et al.* (2009); Laureijs *et al.* (2009); Wang *et al.* (2010)

- Penzias, A. A.; and Wilson, R. W., *Astrophys. J.* **142**, 419 (1965).
- Percival, W. J.; Verde, L.; and Peacock, J. A., *Mon. Not. Roy. Astron. Soc.* **347**, 645 (2004) [arXiv:astro-ph/0306511].
- Percival, W. J.; Cole, S.; Eisenstein, D. J.; Nichol, R. C.; Peacock, J. A.; Pope, A. C.; and Szalay, A. S., *Mon. Not. Roy. Astron. Soc.* **381**, 1053 (2007) [arXiv:0705.3323 [astro-ph]].
- Percival, W. J., *et al.*, *Mon. Not. Roy. Astron. Soc.* **401**, 2148 (2010) [arXiv:0907.1660 [astro-ph.CO]].
- Perlmutter, S., *et al.* [Supernova Cosmology Project Collaboration], *Astrophys. J.* **517**, 565 (1999) [arXiv:astro-ph/9812133].
- Press W.H., Teukolsky S.A., Vetterling W.T., Flannery B.P., 1992, *Numerical recipes in C. The art of scientific computing*, Second edition, Cambridge: University Press.
- Reid, B. A., *et al.*, 2010, *MNRAS*, 404, 60
- Riess, A. G., *et al.* [Supernova Search Team Collaboration], *Astron. J.* **116**, 1009 (1998) [arXiv:astro-ph/9805201].
- Sanchez, A. G.; Baugh, C. M.; and Angulo, R., *Mon. Not. Roy. Astron. Soc.* **390**, 1470 (2008) [arXiv:0804.0233 [astro-ph]].
- Sanchez, A. G.; Crocce, M.; Cabre, A.; Baugh, C. M.; and Gaztanaga, E., arXiv:0901.2570 [astro-ph].
- Seo, H., Eisenstein, D. J., 2003, *ApJ*, 598, 720
- Serra, P.; Cooray, A.; Holz, D. E.; Melchiorri, A.; Pandolfi, S.; Sarkar, D., 2009, *PRD*, 80, 121302
- Smith, R. E., *et al.* [The Virgo Consortium Collaboration], *Mon. Not. Roy. Astron. Soc.* **341**, 1311 (2003) [arXiv:astro-ph/0207664].
- Strauss, M. A., *et al.* [SDSS Collaboration], *Astron. J.* **124**, 1810 (2002) [arXiv:astro-ph/0206225].
- Tegmark, M., *et al.* [SDSS Collaboration], *Astrophys. J.* **606**, 702 (2004) [arXiv:astro-ph/0310725].
- Wang, Y.; Mukherjee, P. 2007, *Phys.Rev.D*, 76, 103533
- Wang, Y., 2009, *PRD*, 80, 123525
- Wang, Y., *et al.*, 2010, *MNRAS*, 409, 737
- Wang, Y.; Chuang, C.-H., & Mukherjee, P. 2011, arXiv:1109.3172
- Zehavi, I., *et al.* [SDSS Collaboration], *Astrophys. J.* **621**, 22 (2005) [arXiv:astro-ph/0411557].
- Zhao, G.-B.; Zhang, X., *PRD*, 81, 043518

APPENDIX A: LN MOCK CATALOGS

One convenient way to generate mock galaxy catalogs for calculating covariance matrix is using lognormal random fields which can approximate the present-day non-linear fluctuation field (Coles & Jones 1991). We create 500 lognormal (LN) density fields (Coles & Jones 1991; Percival, Verde, & Peacock 2004) on a 512^3 grid with box length $4096 h^{-1} \text{Mpc}$. We then draw a random Poisson variable with mean given by the selection functions and lognormal field to create the mock catalogs. We follow the steps described in Percival, Verde, & Peacock (2004) except that we don't cut the input power at 0.25 Nyquist frequency because it makes the restored correlation function deviate from the input one. With a input correlation function, $\xi(r)$, the Gaussian field correlation function is obtained by

$$\xi_G(r) = \ln[1 + \xi(r)], \quad (\text{A1})$$

and this can be Fourier transformed to the power spectrum, $P_G(k)$. A Gaussian density field $\delta_G(r)$ is generated on the grid with this power spectrum, and the corresponding lognormal field is calculated by

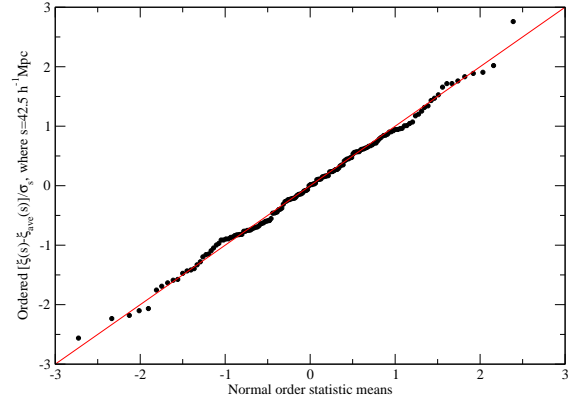


Figure B1. The normality probability plot of the first bins, $40 < s < 45 h^{-1} \text{Mpc}$, of correlation functions from the LasDamas mock catalogs we use for estimating the covariance matrix. The vertical axis is from the ordered values of the first bins from 160 mock catalogs which have been shifted and linearly rescaled to have zero mean and unity variance. The horizontal axis is from the expected values of 160 ordered gaussian random numbers with zero mean and unity variance. That it is an approximate straight line means the bin values are approximately normally distributed.

$$\delta_{LN}(r) = \exp \left[\delta_G(r) - \frac{\sigma_G^2}{2} \right] - 1, \quad (\text{A2})$$

where $1 + \delta_{LN}(r)$ is the lognormal density field which is always positive by definition and σ_G^2 is the variance of the Gaussian density field which can be calculated by

$$\sigma_G^2 = \sum_{i,j,l=1}^{N_{grid}} P_G \left[(k_{x_i}^2 + k_{y_j}^2 + k_{z_l}^2)^{\frac{1}{2}} \right], \quad (\text{A3})$$

where N_{grid} is the number of grid points, $k_{m_n} = \frac{2\pi}{L} \left(n - \frac{N_{grid}}{2} \right)$, L is the box length, and $m = x, y$, or z . Then, the mock catalogs can be constructed by drawing the Poisson random variables with the means given by this lognormal field and the selection function of the galaxy survey.

To compute the correlation function of these mock catalogs, one should create the random data on the same grid as well to cancel out the effect of the finite size of the grid. The input correlation function in this study is the theoretical correlation function with parameters ($\Omega_m = 0.25$, $\Omega_b = 0.04$, $h = 0.7$, $n_s = 1$) which are the same as the input parameters of the LasDamas simulations. We fix $k^* = 0.11$ and the amplitude is adjusted to fit the averaged correlation function from the LasDamas mock catalogs we use. We are not fitting the observed correlation function because we want to find out whether the LN mock catalogs could behave as good as LasDamas mock catalogs while estimating the covariance matrix.

APPENDIX B: NORMALITY TEST

We check the normality of the correlation functions from the LasDamas mock catalogs by showing the normal probability plots of the first and last bin we use (see Fig. B1 and B2). One can tell that they are well described by a normal distribution.

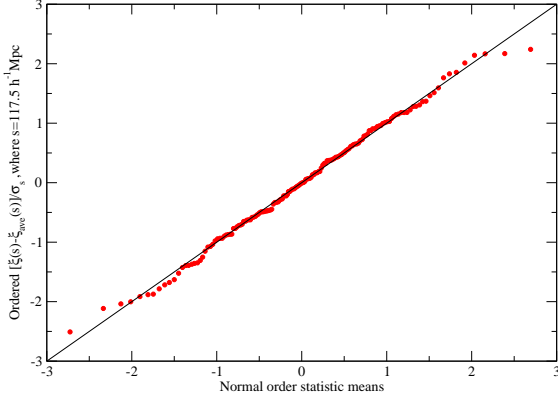


Figure B2. The normality probability plot of the first bins, $115 < s < 120h^{-1}\text{Mpc}$, of correlation functions from the LasDamas mock catalogs we use for estimating the covariance matrix. The vertical axis is from the ordered values of the first bins from 160 mock catalogs which have been shifted and linearly rescaled to have zero mean and unity variance. The horizontal axis is from the expected values of 160 ordered gaussian random numbers with zero mean unity variance. That it is an approximate straight line means the bin values are approximately normally distributed.

APPENDIX C: CMB DISTANCE PRIORS

Wang & Mukherjee (2007) showed that CMB shift parameters (l_a , R), together with $\Omega_b h^2$, provide an efficient and intuitive summary of CMB data as far as dark energy constraints are concerned. It is equivalent to replace $\Omega_b h^2$ with z_* , the redshift to the photon-decoupling surface (Wang 2009).

The CMB shift parameters are defined as (Wang & Mukherjee 2007):

$$R \equiv \sqrt{\Omega_m H_0^2} r(z_*), l_a \equiv \pi r(z_*)/r_s(z_*), \quad (\text{C1})$$

and z_* is the redshift to the photon-decoupling surface given by the fitting formula (Hu and Sugiyama 1996):

$$z_* = 1048 \left[1 + 0.00124(\Omega_b h^2)^{-0.738} \right] \left[1 + g_1(\Omega_m h^2)^{g_2} \right], \quad (\text{C2})$$

where

$$g_1 = \frac{0.0783 (\Omega_b h^2)^{-0.238}}{1 + 39.5 (\Omega_b h^2)^{0.763}} \quad (\text{C3})$$

$$g_2 = \frac{0.560}{1 + 21.1 (\Omega_b h^2)^{1.81}} \quad (\text{C4})$$

The comoving distance to an object at redshift z is given by:

$$r(z) = cH_0^{-1} |\Omega_k|^{-1/2} \text{sinn}[|\Omega_k|^{1/2} \Gamma(z)], \quad (\text{C5})$$

$$\Gamma(z) = \int_0^z \frac{dz'}{E(z')}, \quad E(z) = H(z)/H_0$$

where $\text{sinn}(x) = \sin(x)$, x , $\sinh(x)$ for $\Omega_k < 0$, $\Omega_k = 0$, and $\Omega_k > 0$ respectively; and the expansion rate the universe $H(z)$ is given by

$$H^2(z) \equiv \left(\frac{\dot{a}}{a} \right)^2 \quad (\text{C6})$$

$$= H_0^2 \left[\Omega_m (1+z)^3 + \Omega_r (1+z)^4 + \Omega_k (1+z)^2 + \Omega_X X(z) \right],$$

where $\Omega_m + \Omega_r + \Omega_k + \Omega_X = 1$, and the dark energy density function $X(z)$ is defined as

$$X(z) \equiv \frac{\rho_X(z)}{\rho_X(0)}. \quad (\text{C7})$$

Note that $\Omega_r \ll \Omega_m$, thus the Ω_r term is usually omitted in dark energy studies, since dark energy should only be important at late times.

The comoving sound horizon at redshift z is given by

$$\begin{aligned} r_s(z) &= \int_0^t \frac{c_s dt'}{a} = cH_0^{-1} \int_z^\infty dz' \frac{c_s}{E(z')}, \\ &= cH_0^{-1} \int_0^a \frac{da'}{\sqrt{3(1 + \bar{R}_b a') a'^4 E^2(z')}}, \end{aligned} \quad (\text{C8})$$

where a is the cosmic scale factor, $a = 1/(1+z)$, and $a^4 E^2(z) = \Omega_m(a + a_{\text{eq}}) + \Omega_k a^2 + \Omega_X X(z) a^4$, with $a_{\text{eq}} = \Omega_{\text{rad}}/\Omega_m = 1/(1+z_{\text{eq}})$, and $z_{\text{eq}} = 2.5 \times 10^4 \Omega_m h^2 (T_{\text{CMB}}/2.7 \text{ K})^{-4}$. The sound speed is $c_s = 1/\sqrt{3(1 + \bar{R}_b a)}$, with $\bar{R}_b a = 3\rho_b/(4\rho_\gamma)$, $\bar{R}_b = 31500 \Omega_b h^2 (T_{\text{CMB}}/2.7 \text{ K})^{-4}$. We take $T_{\text{CMB}} = 2.725$.

The redshift of the drag epoch z_d is well approximated by Eisenstein & Hu (1998)

$$z_d = \frac{1291(\Omega_m h^2)^{0.251}}{1 + 0.659(\Omega_m h^2)^{0.828}} \left[1 + b_1(\Omega_b h^2)^{b_2} \right], \quad (\text{C9})$$

where

$$b_1 = 0.313(\Omega_m h^2)^{-0.419} \left[1 + 0.607(\Omega_m h^2)^{0.674} \right], \quad (\text{C10})$$

$$b_2 = 0.238(\Omega_m h^2)^{0.223}. \quad (\text{C11})$$

There are only four independent parameters among these five and n_s is marginalized over in this study. Therefore, there are only three parameters left, $\{l_a, R, z_*\}$. CMB data are included in our analysis by adding the following term to the χ^2 of a given model with $\Delta p_1 = l_a(z_*) - 302.35$, $\Delta p_2 = R(z_*) - 1.728$, and $\Delta p_3 = z_* - 1091.32$:

$$\chi_{\text{CMB}}^2 = \Delta p_i [\text{Cov}_{\text{CMB}}^{-1}(p_i, p_j)] \Delta p_j, \quad (\text{C12})$$

where the inverse covariance matrix of (l_a, R, z_*) from WMAP7 (Komatsu et al. 2010) is given by (Wang, Chuang, & Mukherjee 2011):

$$\text{Cov}_{\text{CMB}}^{-1} = \begin{pmatrix} 1.85710 & 25.9289 & -1.14325 \\ 25.9289 & 5963.26 & -99.3185 \\ -1.14325 & -99.3185 & 2.94429 \end{pmatrix} \quad (\text{C13})$$